Research Square

Preprints are preliminary reports that have not undergone peer review.
They should not be considered conclusive, used to inform clinical practice,
or referenced by the media as validated information.

Spatial heterogeneity of remote sensing-based surface heat conditions and environmental associations in Fuzhou, China: Insights from multiscale geographically weighted regression

Mingxi Tian
Fuzhou University
Yanhong Chen
Fuzhou University Zhicheng College
Yuanbin Cai
t14036@fzu.edu.cn

Fuzhou University
Wenbin Pan
Fuzhou University
Zengxi Fan
Fuzhou University Zhicheng College

Research Article

Keywords: Relative Surface Heat Index (RSHI), surface thermal conditions, spatial heterogeneity, multiscale geographically weighted regression (MGWR), nighttime light, urban green space

Posted Date: November 4th, 2026

DOI: https://doi.org/10.21203/rs.3.rs-11398417/v1

License: This work is licensed under a Creative Commons Attribution 4.0 International License.
Read Full License

Additional Declarations: No competing interests reported.

Spatial heterogeneity of remote sensing-based surface heat conditions and environmental associations in Fuzhou, China: Insights from multiscale geographically weighted regression

Mingxi Tian[1] , Yanhong Chen[2] , Yuanbin Cai [1,*] , Wenbin Pan[1] and Zengxi Fan[2]

[1] College of Environment & Safety Engineering, Fuzhou University, Fuzhou 350108, China; 240627085@fzu.edu.cn (M.T.)

[2] Department of Environmental and Resources Engineering, Fuzhou University Zhicheng College, Fuzhou 350002, China

[*] Correspondence: t14036@fzu.edu.cn; Tel.: +86-133-8591-4526

ABSTRACT

Urban thermal conditions exhibit substantial spatial heterogeneity across cities. This study develops a Relative Surface Heat Index (RSHI) to characterize remote sensing-based surface thermal conditions and examines its spatially heterogeneous and multiscale associations with urban environmental factors in the central urban area of Fuzhou, China. Based on Landsat 9 imagery, RSHI integrates normalized land surface temperature (LST) and the Normalized Difference Water Index (NDWI). Spatial autocorrelation analysis and ordinary least squares (OLS), geographically weighted regression (GWR), and multiscale geographically weighted regression (MGWR) were used to examine the relationships between RSHI and built-up land (BU), water bodies (WB), urban green space (UGS), and nighttime light intensity (NTL). RSHI ranged from 0.236 to 0.910, with a mean of 0.648, and showed significant spatial clustering (Moran's I = 0.452, $p < 0.001$). NTL had the largest global correlation with RSHI ($r = 0.534$), whereas BU, WB, and UGS showed weak global correlations. However, MGWR revealed substantial local variation in these associations. Model performance improved from OLS to GWR and MGWR, with adjusted R^2 increasing from 0.284 to 0.487 and 0.529, respectively. MGWR bandwidths ranged from 52 nearest neighbors for NTL to 2030 for BU, indicating distinct spatial scales of association. These findings highlight the importance of considering spatial heterogeneity and variable-specific spatial scales in urban thermal-environment assessment and planning.

Key words: Relative Surface Heat Index (RSHI); surface thermal conditions; spatial heterogeneity; multiscale geographically weighted regression (MGWR); nighttime light; urban green space

1.Introduction

Urbanization and climate change are increasingly altering the thermal environment of cities, with excessive urban heat becoming an important environmental and public health concern. The intensification of urban development

modifies land-cover composition, surface energy exchange, and local climatic conditions, thereby increasing the likelihood of heat accumulation in densely developed areas. In eastern China, rapid urbanization has been shown to accelerate the increase in urban heat stress, indicating that urban development can amplify the effects of regional climate warming (Luo and Lau, 2018). Exposure to excessive heat is associated with a range of adverse health outcomes, particularly among vulnerable populations, and prolonged heat exposure can increase physiological stress and health risks (Xiang et al., 2014; Ndlovu and Chungag, 2024). Consequently, characterizing the spatial distribution of urban thermal conditions has become increasingly important for understanding urban environmental quality and supporting climate-adaptive planning.

Heat-related environmental conditions, however, are not determined by air or surface temperature alone. Thermal stress is influenced by multiple meteorological variables, including air temperature, humidity, wind speed, and radiation, and different heat-stress indices may produce substantially different estimates of heat exposure (Potchter et al., 2018; Ahn et al., 2024; Rachid and Qureshi, 2023). In particular, humidity can substantially modify the physiological effects of high temperature, and its contribution to heat-related mortality varies among climatic regions (Guo et al., 2024). Recent studies have also highlighted the important role of atmospheric water vapor in shaping heat stress across China (Wang et al., 2024). These findings indicate that urban thermal conditions should be interpreted within a broader environmental context rather than solely from temperature magnitude. This consideration is particularly relevant for humid subtropical coastal cities, where surface thermal conditions are closely associated with both temperature and moisture-related characteristics.

Satellite remote sensing has become one of the most widely used approaches for characterizing urban thermal environments because it provides spatially continuous observations of land surface temperature (LST) at relatively fine spatial resolutions. LST-based surface urban heat island studies have substantially improved the understanding of the spatial and temporal characteristics of urban thermal environments and their relationships with land-cover and urban morphological factors (Zhou et al., 2024; Shi et al., 2025). However, LST primarily represents the thermal state of the land surface and does not directly describe human thermal perception or physiological heat stress. Therefore, LST-based analyses should not be regarded as direct substitutes for human biometeorological indices (Potchter et al., 2018; Ahn et al., 2024). At the same time, remote-sensing studies have demonstrated that urban surface thermal conditions are closely associated with the spatial configuration of built-up land, vegetation, and water bodies. In Fuzhou, previous studies have documented the effects of urban expansion and land-cover transformation on LST (Cai et al., 2016a; Cai et al., 2016b; Zheng et al., 2019), while green spaces and water bodies have been shown to provide cooling effects (Cai et al., 2019; Cai et al., 2022; Shen et al., 2022). However, the magnitude and spatial extent of these relationships can vary with landscape configuration, season, and surrounding urban context (He et al., 2024; Yan et al., 2024). Recent research has further emphasized that the

thermal-regulation performance of blue-green infrastructure depends on spatial configuration and the balance between cooling supply and urban thermal demand (Guan et al., 2025; Ma et al., 2025). These findings suggest that an integrated characterization of relative surface thermal conditions may provide complementary information to conventional LST-based assessments, particularly in humid urban environments.

Importantly, the relationships between urban thermal conditions and environmental factors are not necessarily spatially uniform. Yang et al. (2022) investigated the dominant factors of LST in urban Fuzhou using ordinary least squares (OLS), geographically weighted regression (GWR), and multiscale geographically weighted regression (MGWR), and demonstrated substantial spatial heterogeneity in the relationships between LST and environmental factors. Similar spatially varying relationships have also been reported in other urban thermal-environment studies using geographically weighted approaches (Gao et al., 2022; Xu et al., 2024). These studies demonstrate that city-wide relationships may not adequately represent the spatial complexity of urban thermal environments. Nevertheless, an important issue remains insufficiently explored: whether weak or insignificant global associations necessarily indicate weak relationships throughout the city.

A near-zero global correlation does not necessarily imply the absence of a meaningful spatial relationship. When the direction or strength of an association varies across space, positive and negative local relationships may offset each other when aggregated at the city-wide scale, resulting in a weak global association. This issue is particularly relevant to urban environmental variables such as built-up land, vegetation, and water bodies, whose relationships with surface thermal conditions may depend on local urban form, landscape configuration, and surrounding land-cover context. Consequently, distinguishing between global associations and spatially varying local associations is important for determining whether an apparently weak city-wide relationship represents a genuinely weak association or masks substantial spatial heterogeneity.

Geographically weighted regression (GWR) provides a framework for addressing this issue by allowing regression coefficients to vary spatially, thereby revealing local variations in the associations between response and explanatory variables. However, conventional GWR generally applies a common bandwidth to all explanatory variables, implicitly assuming that different environmental processes operate at the same spatial scale. In contrast, multiscale geographically weighted regression (MGWR) allows each explanatory variable to have its own bandwidth, providing a framework for identifying both spatial heterogeneity and variable-specific spatial scales (Oshan et al., 2019). This distinction is particularly relevant to urban thermal research because different environmental and anthropogenic processes may operate over substantially different spatial ranges. Thus, combining global regression with GWR and MGWR can provide a more complete perspective by distinguishing overall associations, local spatial variation, and variable-specific spatial scales.

Fuzhou, a humid subtropical coastal city in southeastern China, provides an appropriate case for investigating these issues because of its complex

urban-blue-green landscape and rapidly changing urban environment.Previous studies have examined the spatial heterogeneity of land surface temperature (LST) and its relationships with urban environmental factors in Fuzhou (Yang et al., 2022;Zheng et al., 2018; Du et al., 2020; Lin et al., 2023), as well as the thermal effects of urban green spaces, water bodies, and land-cover change (Cai et al., 2019; Cai et al., 2022; Zheng et al., 2019). These studies provide an important basis for understanding the urban thermal environment, but they also highlight the need to distinguish the spatial pattern of a composite surface indicator from the spatial relationships associated with individual environmental variables. In particular, it remains important to determine whether weak city-wide associations between surface thermal conditions and landscape variables conceal locally contrasting relationships, and whether these relationships are characterized by different spatial scales. Addressing these questions requires an analysis that jointly examines global associations, local coefficient variation, and variable-specific spatial scales, while explicitly considering the sensitivity of the composite indicator to alternative construction choices.

To address these issues, this study develops a Relative Surface Heat Index (RSHI) as a study-specific indicator of relative surface thermal and moisture-related conditions in the central urban area of Fuzhou, China. The study combines spatial autocorrelation analysis with OLS, GWR, and MGWR to investigate the spatial organization of RSHI and its associations with built-up land (BU), water bodies (WB), urban green space (UGS), and nighttime light intensity (NTL). Specifically, this study addresses three questions: (1) How is RSHI spatially distributed, and to what extent does it exhibit spatial clustering? (2) Do weak global associations between RSHI and environmental variables conceal spatially heterogeneous local relationships? (3) To what extent do the estimated spatial scales of these associations differ among explanatory variables, and how sensitive are the identified RSHI patterns to alternative index specifications? By addressing these questions, the study provides a spatially explicit assessment of the relationships between a composite surface indicator and urban environmental characteristics, while clarifying the interpretation and sensitivity of the index.

2 .Materials and Methods

2.1 Study area

Fuzhou City (118°08′-120°31′E, 25°15′-26°39′N), the capital of Fujian Province, is located in southeastern China, along the lower reaches of the Min River and the coastal region. It has a typical subtropical monsoon climate characterized by high temperature, abundant precipitation, and high humidity. The annual precipitation ranges from 900 to 2100 mm. The city is located within a river-estuary basin, where the combined effects of coastal climate, complex terrain, and intensive human activities contribute to a unique urban thermal environment.

In this study, the central urban area of Fuzhou was selected as the study area (Fig. 1). According to the urban spatial planning framework of Fuzhou, the central urban area includes all districts under the jurisdiction of Fuzhou City (excluding Huanxi

Town, Shoushan Township, and Rixi Township in Jin'an District), as well as several towns in surrounding counties, including Jingxi, Shangjie, Nanyu, Nantong, Shanggan, Qingkou, and Xiangqian towns in Minhou County, and Guantou Town in Lianjiang County. The total area of the study area is approximately 2213 km².

As a rapidly urbanizing coastal city in southeastern China, Fuzhou has experienced continuous population growth and land-use transformation in recent decades. The expansion of impervious surfaces and increasing human activity have contributed to changes in the urban thermal environment. Fuzhou therefore provides a useful case study for examining the spatial distribution of relative surface thermal conditions and the spatially varying associations between these conditions and urban environmental factors.

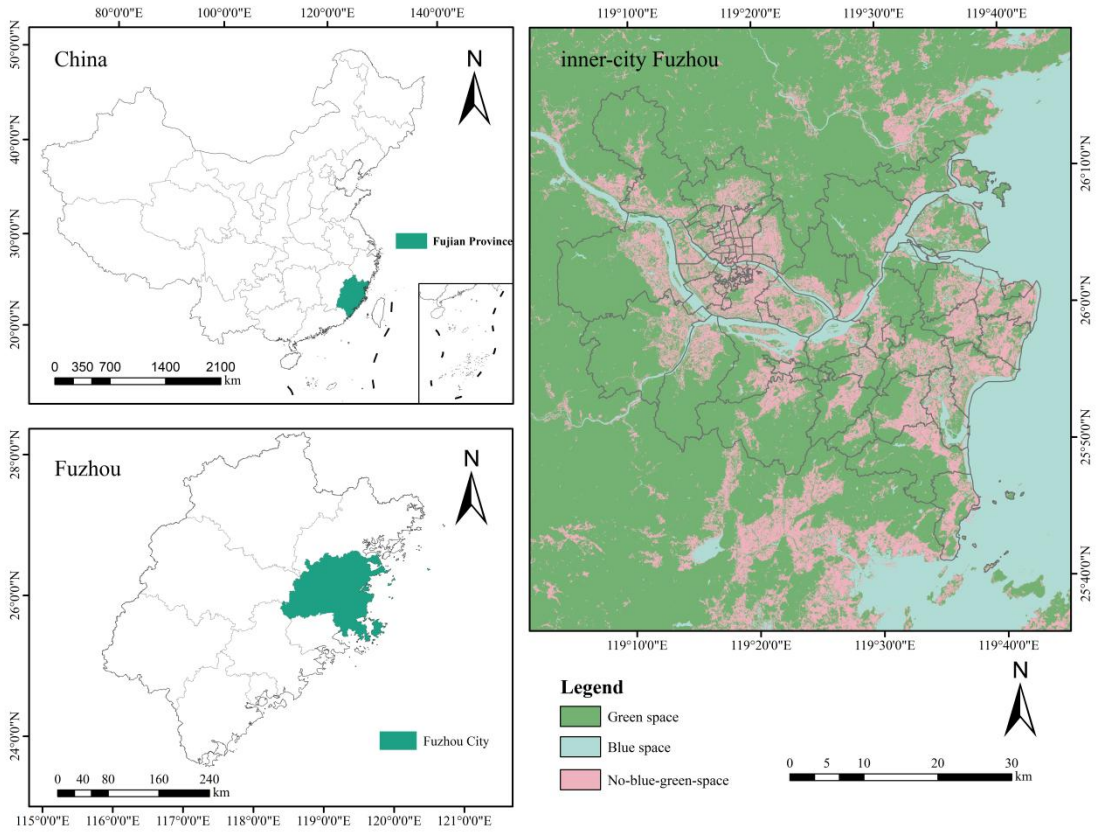


Fig.1.Overview of the study area

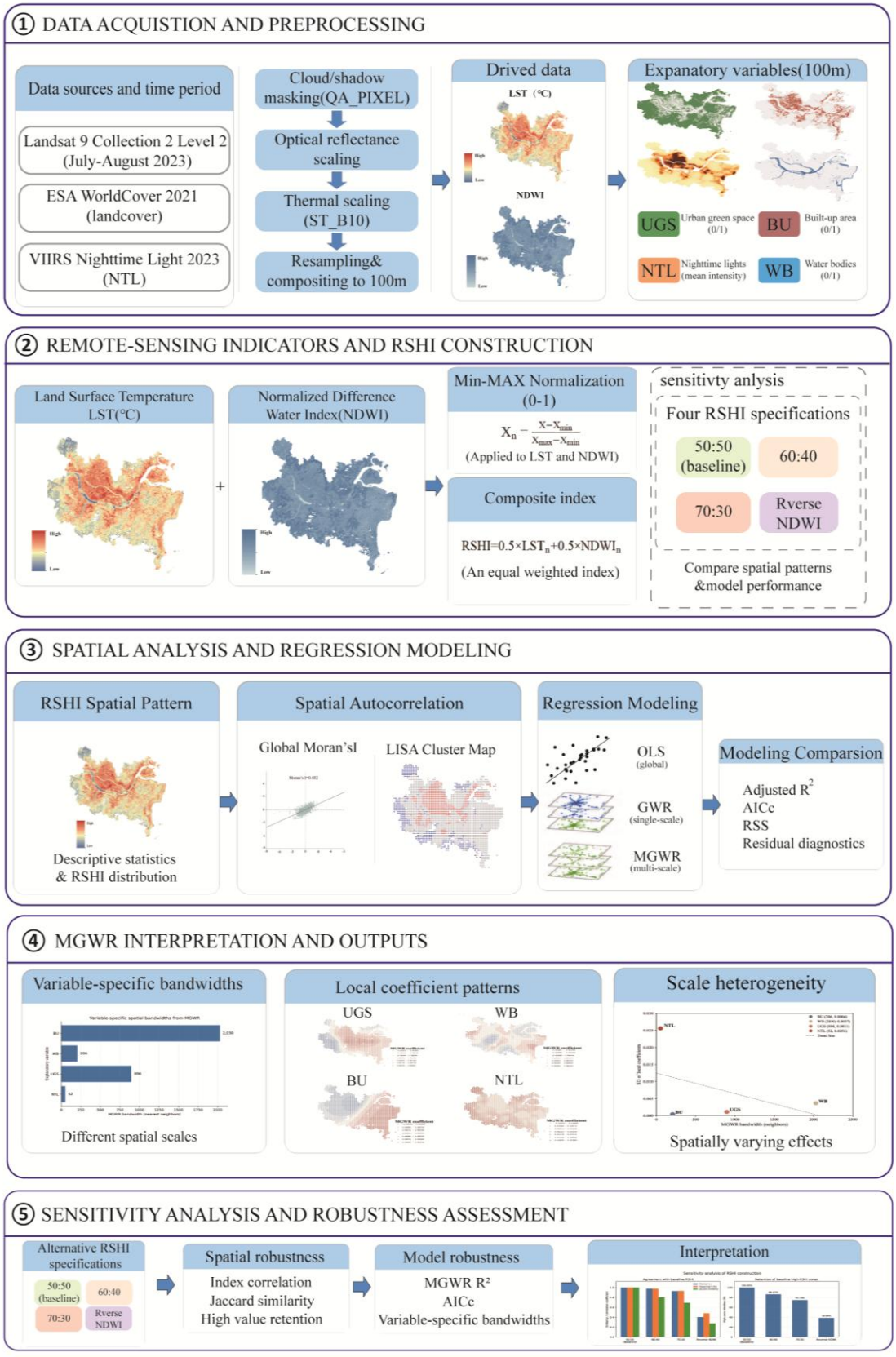


Fig.2.Analytical framework of this study

2.2 Data sources and preprocessing

Table 1.Summary of datasets used in this study

Data	Source	Resolution	Year	Purpose
Landsat 9 Surface Reflectance	USGS / Google Earth Engine	30 m	2023	Retrieval of LST and calculation of RSHI
ESA WorldCover	ESA WorldCover v200	10 m	2021	Extraction of green space (UGS) and water body (WB)
Nighttime Light (NTL)	VIIRS VNL V2	500m	2023	Socioeconomic indicator

The datasets used in this study are summarized in Table 1. Landsat 9 Surface Reflectance imagery was acquired from the USGS/Google Earth Engine platform for the year 2023 to retrieve LST and calculate RSHI.

Multiple datasets were integrated to characterize the thermal environment and urban landscape characteristics in Fuzhou. The datasets included Landsat 9 satellite imagery, ESA WorldCover land cover data, nighttime light (NTL) data. Detailed information on the datasets is summarized in Table 1.

To ensure spatial consistency among datasets, all raster datasets were projected to a common coordinate reference system and resampled to a spatial resolution of 100 m. A regular 100 m × 100 m grid was initially used for raster alignment and data preprocessing. Subsequently, the processed variables were aggregated to 1 km × 1 km grid cells, which were used as the basic analytical units for spatial autocorrelation and regression analyses.The centroid coordinates of each 1 km × 1 km grid cell were extracted for subsequent spatial analysis and geographically weighted regression modeling.

Landsat 9 Operational Land Imager and Thermal Infrared Sensor (OLI/TIRS) Level-2 surface temperature products were obtained from the Google Earth Engine (GEE) platform. Cloud-free images acquired during July-August were selected to represent summer thermal conditions. The quality assessment band (QA_PIXEL) was used to remove cloud and cloud-shadow pixels. Land surface temperature (LST) was extracted from the thermal infrared band and converted into degrees Celsius.

The Normalized Difference Water Index (NDWI) was calculated from the green and near-infrared bands to represent a remotely sensed surface-moisture-related characteristic. NDWI is not a direct measurement of atmospheric humidity or human heat exposure.

ESA WorldCover v200 2021 land cover data with a spatial resolution of 10 m were used to derive urban landscape indicators. Land cover classes were reclassified into vegetation, water bodies, and built-up surfaces. The proportions of green space, blue space, and built-up areas within each 1 km grid were calculated to represent urban ecological and morphological characteristics.

Nighttime light intensity data were used as a proxy for human activity intensity and urbanization level. The NTL data were resampled and spatially aggregated to the 1 km grid scale, and the mean value within each grid cell was calculated.

After preprocessing, the variables were integrated into a unified dataset at the 1 km grid scale. Grid-cell centroids were extracted for the spatial autocorrelation and geographically weighted regression analyses.

2.3 Construction of the Relative Surface Heat Index (RSHI)

The Relative Surface Heat Index (RSHI) was developed as a study-specific composite indicator of relative surface thermal and moisture-related conditions using Landsat 9 imagery. It combines land surface temperature (LST) and the Normalized Difference Water Index (NDWI) to represent two complementary dimensions of the urban surface environment. The index characterizes spatial differences in the weighted combination of these components; it is not intended to quantify human thermal comfort, physiological heat stress, or health risk.

The NDWI was calculated from green and near-infrared surface reflectance:

$$NDWI=\frac{Green-NIR}{Green+NIR} \quad (1)$$

where Green and NIR denote the green and near-infrared surface reflectance bands, respectively.

LST and NDWI were independently normalized using min-max normalization:

$$X_n=\frac{X-X_{min}}{X_{max}-X_{min}} \quad (2)$$

where X_n is the normalized value of variable X, and X_{min} and X_{max} represent the minimum and maximum values of X, respectively.

The RSHI was then constructed by assigning equal weights to the normalized LST and NDWI:

$$RSHI=0.5\times LST_n+0.5\times NDWI_n \quad (3)$$

where LST_n and $NDWI_n$ denote normalized LST and NDWI, respectively. Equal weights were adopted as a transparent baseline specification rather than as an empirically optimized weighting scheme. Higher RSHI values therefore indicate higher composite values of normalized LST and NDWI; they do not necessarily indicate higher LST alone, drier surface conditions, or greater human heat risk. Interpretation focuses on the spatial distribution and associations of this composite surface thermal-moisture indicator.

The use of a moisture-related indicator is also consistent with previous research in Fuzhou showing that water and green spaces play important but spatially differentiated roles in regulating the urban thermal environment (Cai et al., 2022).

The RSHI raster was generated at a spatial resolution of 100 m and subsequently aggregated to 1 km × 1 km grid cells. The mean RSHI value within each grid cell was used as the dependent variable in the subsequent spatial autocorrelation and regression analyses.

2.4 Sensitivity analysis

To examine the sensitivity of the derived spatial patterns to the construction of RSHI, the 50:50 weighting scheme was retained as the baseline specification, and two

alternative positive weighting schemes (60:40 and 70:30 for normalized LST and NDWI, respectively) were evaluated. An additional scenario reversing the direction of the normalized NDWI component was included as a directional sensitivity test. These scenarios were designed to assess the dependence of the results on index specification rather than to identify an optimal weighting scheme.

Spatial-pattern sensitivity was assessed by calculating Pearson and Spearman correlation coefficients between the baseline and alternative RSHI rasters using common valid pixels. The spatial overlap of high-value areas was evaluated using the Jaccard similarity coefficient under a consistent classification threshold. Model sensitivity was assessed by comparing MGWR goodness-of-fit statistics, variable-specific adaptive bandwidths, and local coefficient distributions across the four scenarios. The 50:50 specification was retained for the main analysis to ensure consistency with the original study design, while the sensitivity results were used to evaluate the robustness and limitations of the resulting spatial interpretations.

The alternative weighting scenarios were designed to assess the sensitivity of the RSHI spatial pattern to the relative contributions of normalized LST and NDWI, whereas the reversed-NDWI scenario was used to examine the dependence of the composite index on the direction assigned to its moisture-related component. These scenarios serve different purposes: the former evaluates sensitivity to weight selection, while the latter evaluates sensitivity to component direction. The 50:50 specification was retained as the baseline for comparison and was not treated as an empirically optimized weighting scheme.

2.5 Spatial autocorrelation analysis

Spatial autocorrelation analysis was conducted to assess the spatial dependence and clustering structure of RSHI. Global Moran's I was first calculated to evaluate the overall spatial autocorrelation of RSHI:

$$I=\frac{n}{S_0}\frac{\sum_{i=1}^{n}\sum_{j=1}^{n} w_{ij}(x_i-\overline{x})(x_j-\overline{x})}{\sum_{i-1}^{n}(x_i-\overline{x})^2} \quad (4)$$

where nn is the number of spatial units, x_i and x_j are the RSHI values of spatial units i and j, respectively, $\overline{x}$ is the mean RSHI value, and w_{ij} is the spatial weight between units i and j. S_0 is the sum of all spatial weights, defined as

$$S_0=\sum_{i=1}^{n}\sum_{j=1}^{n} w_{ij}$$

Positive Moran's I values indicate positive spatial autocorrelation, whereby spatial units with similar RSHI values tend to be located near one another, whereas negative values indicate spatial dispersion.

Local Indicators of Spatial Association (LISA) were subsequently used to identify local clusters and spatial outliers. The Local Moran's I statistic was calculated as

$$I_i=\frac{x_i-\overline{x}}{m_2}\sum_{j=1}^{n} w_{ij}(x_j-\overline{x}) \quad (5)$$

where I_i represents the local spatial association statistic for spatial unit i, and

$$m_2=\frac{1}{n}\sum_{i=1}^{n}(x_i-\overline{x})^2$$

Based on the relationship between each grid cell and its neighboring cells, significant local associations were classified into four categories: High-High (HH), Low-Low (LL), High-Low (HL), and Low-High (LH). HH and LL clusters represent areas where relatively high or low RSHI values are surrounded by neighboring grid cells with similar values, whereas HL and LH indicate local spatial outliers.

A first-order Queen contiguity matrix was used to define spatial neighbors among adjacent 1 km × 1 km grid cells. Statistical significance was assessed using 999 random permutations with a significance level of $p<0.05$. All spatial autocorrelation analyses were performed in GeoDa 1.22.

2.6 OLS, GWR, and MGWR models

To investigate the relationships between urban environmental factors and RSHI, Ordinary Least Squares (OLS), Geographically Weighted Regression (GWR), and Multiscale Geographically Weighted Regression (MGWR) models were sequentially applied. The explanatory variables included built-up area (BU), water bodies (WB), urban green space (UGS), and nighttime light intensity (NTL).

Pearson correlation analysis was first conducted to characterize the global linear associations between RSHI and the explanatory variables:

$$r_{xy}=\frac{\sum_{i=1}^{n}(x_i-\overline{x})(y_i-\overline{y})}{\sqrt{\sum_{i=1}^{n}(x_i-\overline{x})^2\sum_{i=1}^{n}(y_i-\overline{y})^2}} \quad (6)$$

where r_{xy} is the Pearson correlation coefficient between variables x and y, and $\overline{x}$ and $\overline{y}$ are their respective means.

Variance Inflation Factor (VIF) was subsequently used to assess multicollinearity among the explanatory variables:

$$VIF_j=\frac{1}{1-R_j^2} \quad (7)$$

where R_j^2 is the coefficient of determination obtained by regressing the j-th explanatory variable against all other explanatory variables.

Ordinary Least Squares

The OLS model was specified as

$$RSHI_i=\beta_0+\beta_1 BU_i+\beta_2 WB_i+\beta_3 UGS_i+\beta_4 NTL_i+\varepsilon_i \quad (8)$$

where $RSHI_i$ is the RSHI value of grid cell i, β_0 is the intercept, β_k represents the global coefficient of the k-th explanatory variable, and ε_i is the residual term. OLS provides a global estimate of the average linear association between RSHI and the explanatory variables across the study area.

Geographically Weighted Regression

To account for spatial non-stationarity, GWR was subsequently applied by allowing regression coefficients to vary across geographical locations:

$$RSHI_i = \beta_0(u_i, v_i) + \sum_{k=1}^{p} \beta_k(u_i, v_i)X_{ik} + \varepsilon_i \quad (9)$$

where (u_i,v_i) denotes the spatial coordinates of grid cell i, X_{ik} represents the kk-th explanatory variable, and $\beta_k(u_i, v_i)$ is the location-specific regression coefficient.

An adaptive bi-square kernel was used to define the spatial weights, and the optimal bandwidth was selected by minimizing the corrected Akaike Information Criterion (AICc). The adaptive bandwidth was defined in terms of neighboring observations, allowing the effective spatial scale to adjust to variations in sampling density.

Multiscale Geographically Weighted Regression

Although GWR allows coefficients to vary spatially, it applies a common bandwidth to all explanatory variables. MGWR relaxes this assumption by allowing each explanatory variable to have its own bandwidth (Oshan et al., 2019):

$$RSHI_i = \beta_0(u_i, v_i) + \sum_{k=1}^{p} \beta_k(u_i, v_i; b_k)X_{ik} + \varepsilon_i \quad (10)$$

where b_k denotes the variable-specific bandwidth associated with the k-th explanatory variable. Thus, MGWR allows different RSHI-environment relationships to be estimated over different spatial scales.

The variable-specific bandwidths were interpreted as the number of nearest-neighbor observations used in the adaptive kernel rather than as fixed physical distances. Consequently, the estimated bandwidths represent the relative spatial scale of the modeled associations and should not be interpreted as direct cooling distances.

Model evaluation

The performance of the OLS, GWR, and MGWR models was evaluated using the residual sum of squares (RSS), adjusted coefficient of determination (Adjusted R^2), and corrected Akaike Information Criterion (AICc).

The RSS was calculated as

$$RSS = \sum_{i=1}^{n}(y_i - \hat{y}_i)^2 \quad (11)$$

where y_i and $\hat{y}_i$ are the observed and predicted values for grid cell i, respectively.

The adjusted coefficient of determination was calculated as

$$R^2_{adj} = 1 - \frac{(1-R^2)(n-1)}{n-p-1} \quad (12)$$

where R^2 is the coefficient of determination, n is the number of observations, and p is the number of explanatory variables.

The corrected Akaike Information Criterion was calculated as

$$AICc = AIC + \frac{2K(K+1)}{n-K-1} \quad (13)$$

where K is the number of estimated parameters. Higher Adjusted R^2 and lower RSS and AICc indicate better model fit.

OLS and GWR analyses were conducted in R using the GWmodel package, whereas MGWR was implemented using the MGWR 2.2 software package in Python.

3.Results

3.1 Spatial distribution and statistical characteristics of RSHI

The spatial distribution and statistical characteristics of the Relative Surface Heat Index (RSHI) are shown in Fig.3.RSHI exhibited substantial spatial variability across the central urban area of Fuzhou. The values ranged from approximately 0.236 to 0.910, with a mean of 0.648 and a standard deviation of 0.043. The frequency distribution indicates that RSHI values were concentrated mainly within the intermediate range rather than being uniformly distributed across the full range.

The Jenks classification further revealed an uneven distribution of RSHI classes. The third and fourth classes accounted for approximately 32.26% and 31.15% of the study area, respectively, together representing 63.40% of the total area. In contrast, the lowest RSHI class accounted for only 3.03%, while the highest class occupied 17.01%. This distribution indicates that most of the study area fell within the intermediate classes of the composite RSHI, while the lowest and highest index classes occupied comparatively smaller areas. Because the RSHI integrates normalized LST and NDWI with equal weights, these classes represent relative differences in the combined surface thermal-moisture indicator rather than temperature-defined thermal classes alone.

The spatial pattern of RSHI showed clear geographic differentiation. Relatively high RSHI values were mainly distributed within densely developed urban areas, while relatively low values were more frequently observed in areas with greater coverage of vegetation and water bodies. The east-west spatial profile also indicated systematic variation in RSHI across the study area, with mean values along the profile ranging from approximately 0.592 to 0.673. These spatial contrasts were broadly consistent with the distributions of built-up land, urban green space, water bodies, and nighttime light intensity shown in Fig. 5.

However, the spatial correspondence between RSHI and individual explanatory variables should not be interpreted as evidence of a uniform relationship across the study area. For example, areas with similar levels of built-up development may exhibit different RSHI values depending on their surrounding landscape composition and human activity intensity. This spatial variation provides the basis for subsequent spatial autocorrelation and geographically weighted regression analyses.

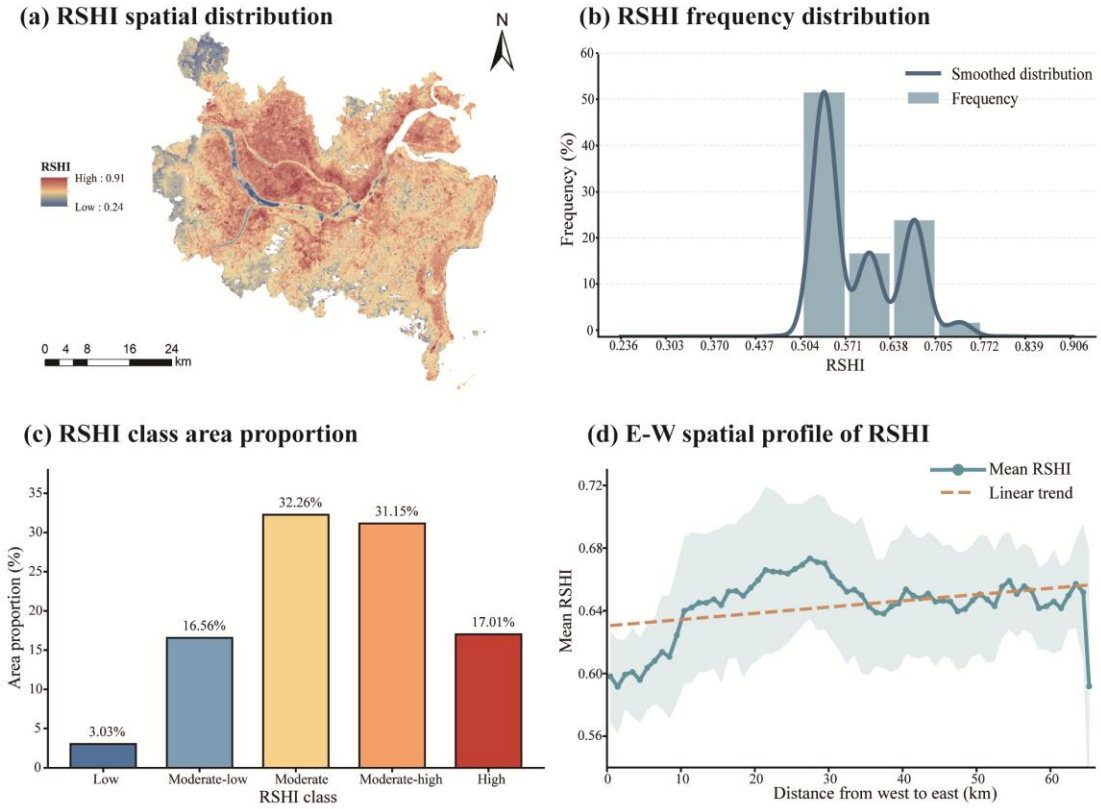


Fig. 3 Spatial pattern and statistical characteristics of RSHI. (a) Spatial distribution of RSHI.(b) Frequency distribution of RSHI.(c) Area proportion of RSHI classes. (d) E-W spatial profile of RSHI.

3.2 Spatial distribution and descriptive statistics of explanatory variables

Table 2.Descriptive statistics of RSHI and explanatory variables

Variable	Mean	SD	Min	Max
RSHI	0.648	0.043	0.236	0.910
Built-up land(BU)	0.167	0.231	0.000	0.910
Water bodies (WB)	0.067	0.169	0.000	1.000
Urban green space ratio (UGS)	0.637	0.331	0.000	1.000
Nighttime light (NTL)	9.565	13.425	0.000	81.535

Table 3.Correlation matrix and multicollinearity diagnostics

Variable	RSHI	BU	WB	UGS	NTL	VIF
RSHI	1.000	-0.021	0.014	0.027	0.534	—
BU	-0.021	1.000	-0.055	-0.495	-0.025	1.332
WB	0.014	-0.055	1.000	-0.018	0.029	1.007
UGS	0.027	-0.495	-0.018	1.000	0.017	1.328
NTL	0.534	-0.025	0.029	0.017	1.000	1.001

The explanatory variables exhibited distinct spatial distributions across the study area (Fig. 5; Table 2). BU had a mean proportion of 0.167, with values ranging from 0 to 0.910, whereas UGS had a substantially higher mean proportion of 0.637. WB occupied a relatively smaller proportion of the study area, with a mean value of 0.067. NTL had a mean value of 9.565 and a standard deviation of 13.425, indicating considerable spatial variation in nighttime light intensity.

The spatial distributions further showed that BU and NTL were concentrated mainly in densely developed urban areas, whereas WB followed the major river and water-network structure. UGS was more broadly distributed and formed spatially heterogeneous green-space patterns across the urban area. These contrasting distributions indicate that the four explanatory variables represent different components of the urban landscape and human activity system rather than a single spatial process.

The correlation matrix revealed an important difference between the global relationships of RSHI with the explanatory variables (Table 3). RSHI showed a moderate positive correlation with NTL ($r = 0.534$), whereas the correlations with BU ($r = -0.021$), WB ($r = 0.014$), and UGS ($r = 0.027$) were close to zero. Thus, NTL showed the strongest global linear association with RSHI among the four explanatory variables.

At the same time, BU and UGS exhibited a moderate negative correlation ($r = -0.495$), indicating that areas with a higher proportion of built-up land tended to have lower proportions of urban green space. In contrast, the correlations among the remaining explanatory variables were weak. The VIF values ranged from 1.001 to 1.332, indicating that the explanatory variables did not exhibit problematic multicollinearity. Therefore, the spatial heterogeneity identified in the subsequent GWR and MGWR analyses is unlikely to be primarily attributable to severe linear dependence among the predictors.

Importantly, the near-zero global correlations between RSHI and BU, WB, and UGS do not necessarily indicate the absence of spatially varying relationships. Rather, they suggest that positive and negative local associations may be partially offset when aggregated into a single global correlation coefficient. This distinction becomes particularly relevant in the MGWR results.

3.3 Spatial autocorrelation and local clustering of RSHI

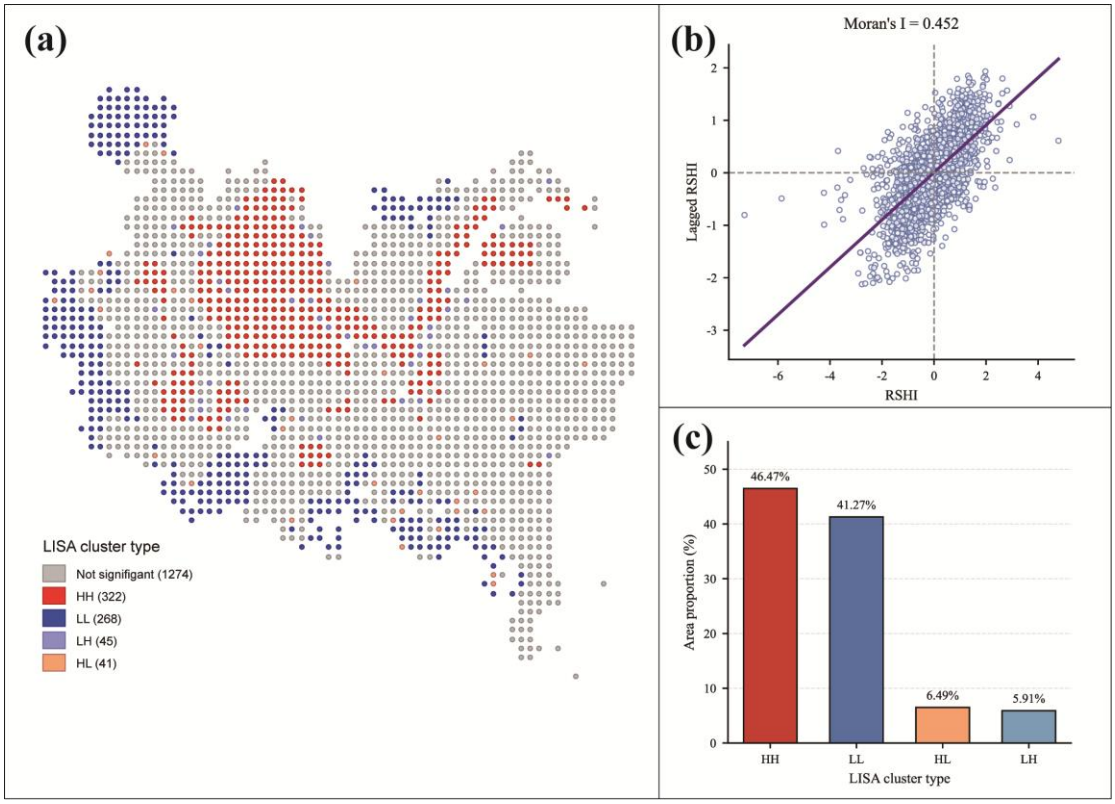


Fig. 4. Spatial autocorrelation and local spatial clustering patterns of RSHI in Fuzhou. (a) Moran scatter plot; (b) LISA cluster map; (c) area proportions of different LISA cluster types.

The spatial autocorrelation analysis demonstrated that RSHI was not randomly distributed across the study area. Global Moran's I was 0.452 with $p < 0.001$, indicating significant positive spatial autocorrelation. Therefore, areas with relatively similar RSHI values tended to occur near one another, and the spatial pattern observed in Fig. 3 contained a statistically significant spatial structure.

The LISA analysis provided further information on the local configuration of this spatial dependence (Fig. 4). HH clusters were primarily located within highly developed urban areas, corresponding to local concentrations of relatively high RSHI values surrounded by similarly high values. In contrast, LL clusters were mainly distributed in areas associated with more extensive vegetation and water bodies, indicating local concentrations of relatively low RSHI values.

HL and LH observations were comparatively scattered and were mainly located around transition zones between highly developed and relatively ecological landscapes. These locations represent local departures from the surrounding spatial pattern rather than dominant regional structures. The coexistence of HH and LL clusters, together with the limited distribution of HL and LH observations, indicates that the positive global Moran's I was mainly associated with spatially coherent high- and low-value regions rather than being driven by isolated spatial outliers.

Overall, the Moran's I and LISA results establish that RSHI exhibits both global spatial dependence and localized clustering structures. This spatial dependence provides a statistical basis for moving beyond a global regression framework and

examining whether the relationships between RSHI and its explanatory variables vary geographically.

3.4 Performance comparison of OLS, GWR, and MGWR

The performance of the OLS, GWR, and MGWR models is summarized in Table 5 and Fig. 6. The three models showed a progressive improvement in explanatory performance as spatial heterogeneity was incorporated into the regression framework.

The OLS model achieved an adjusted R^2 of 0.284, with an RSS of 2.753 and an AICc of −7889.133. Among the OLS coefficients, NTL was positively associated with RSHI and was statistically significant (coefficient = 0.0017, $p < 0.001$), whereas BU, WB, and UGS were not statistically significant at the global level. This result is consistent with the correlation analysis, in which NTL showed the strongest global association with RSHI.

Allowing coefficients to vary spatially in the GWR model substantially improved model performance. The adjusted R^2 increased from 0.284 to 0.487, while RSS decreased from 2.753 to 1.697 and AICc decreased from −7889.133 to −8415.344. The reduction in RSS from OLS to GWR was approximately 38.4%. These changes indicate that a considerable proportion of the variation not captured by the global model could be represented by allowing regression relationships to vary across space.

MGWR produced a further improvement over GWR. The adjusted R^2 increased from 0.487 to 0.529, while RSS decreased from 1.697 to 1.650 and AICc decreased from −8415.344 to −8548.967. The additional reduction in RSS from GWR to MGWR was relatively modest (approximately 2.8%) compared with the improvement from OLS to GWR, but the consistent changes in adjusted R^2, RSS, and AICc indicate that allowing different explanatory variables to operate at different spatial scales provided additional explanatory flexibility.

Model comparison showed that allowing regression relationships to vary spatially substantially improved the representation of RSHI compared with the global OLS model. Adjusted R^2 increased from 0.284 in OLS to 0.487 in GWR, accompanied by a decrease in RSS from 2.753 to 1.697. MGWR further improved the model fit, with adjusted R^2 increasing to 0.529 and RSS decreasing to 1.650. AICc also decreased from −8415.344 in GWR to −8548.967 in MGWR. The additional improvement from GWR to MGWR was smaller than that from OLS to GWR, but the consistent changes in the reported fit statistics support the use of variable-specific bandwidths to represent the spatially heterogeneous associations between RSHI and the explanatory variables.

Table 4.Global regression results from the OLS model

Variable	Coefficient	Std.Error	t	p
Intercept	0.630	0.002	260.27	<0.001
BU	0.0002	0.004	0.05	0.960
WB	-0.0002	0.005	-0.05	0.962
UGS	0.0023	0.003	0.84	0.402
NTL	0.0017	0.0001	28.76	<0.001

Table 5.Performance comparison of the OLS, GWR, and MGWR models

Model	Adj. R^2	AICc	RSS
OLS	0.284	-7889.133	2.753
GWR	0.487	-8415.344	1.697
MGWR	0.529	-8548.967	1.650

3.5 Spatial heterogeneity and multiscale characteristics of explanatory-variable associations

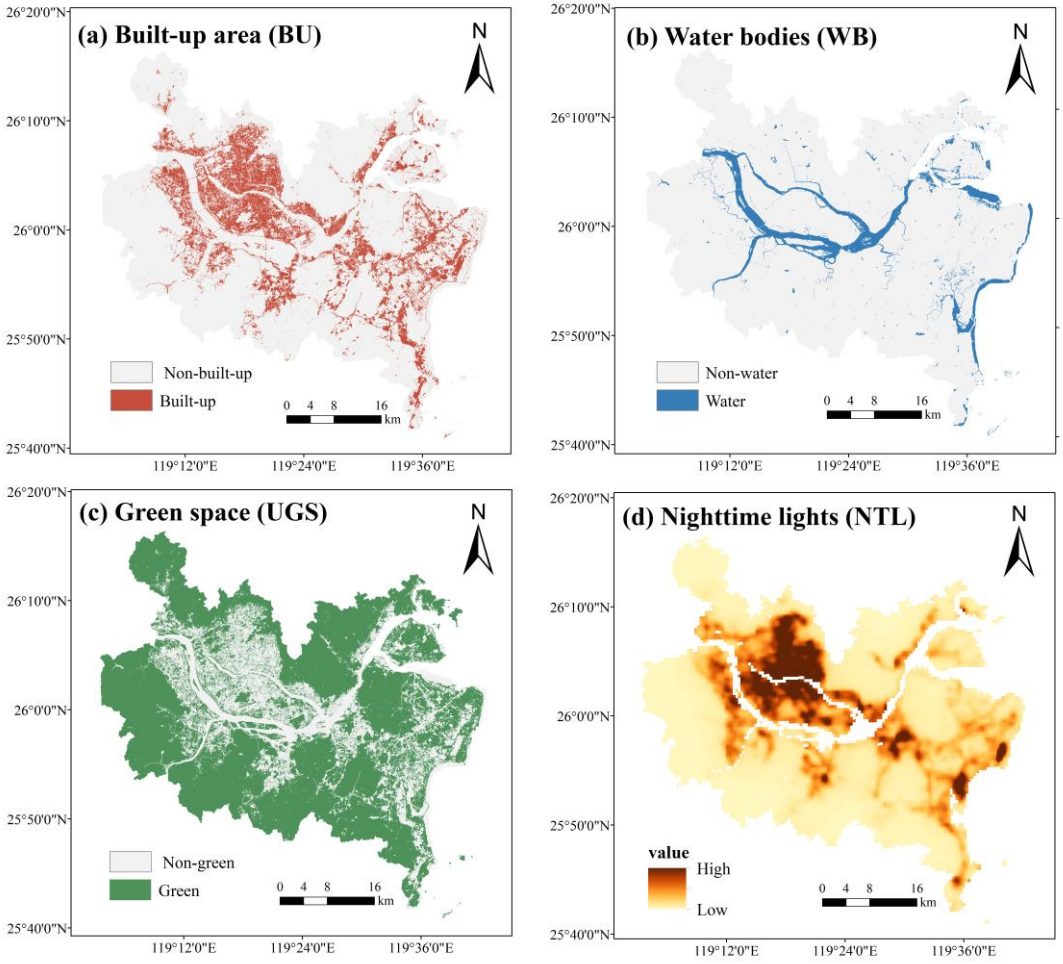
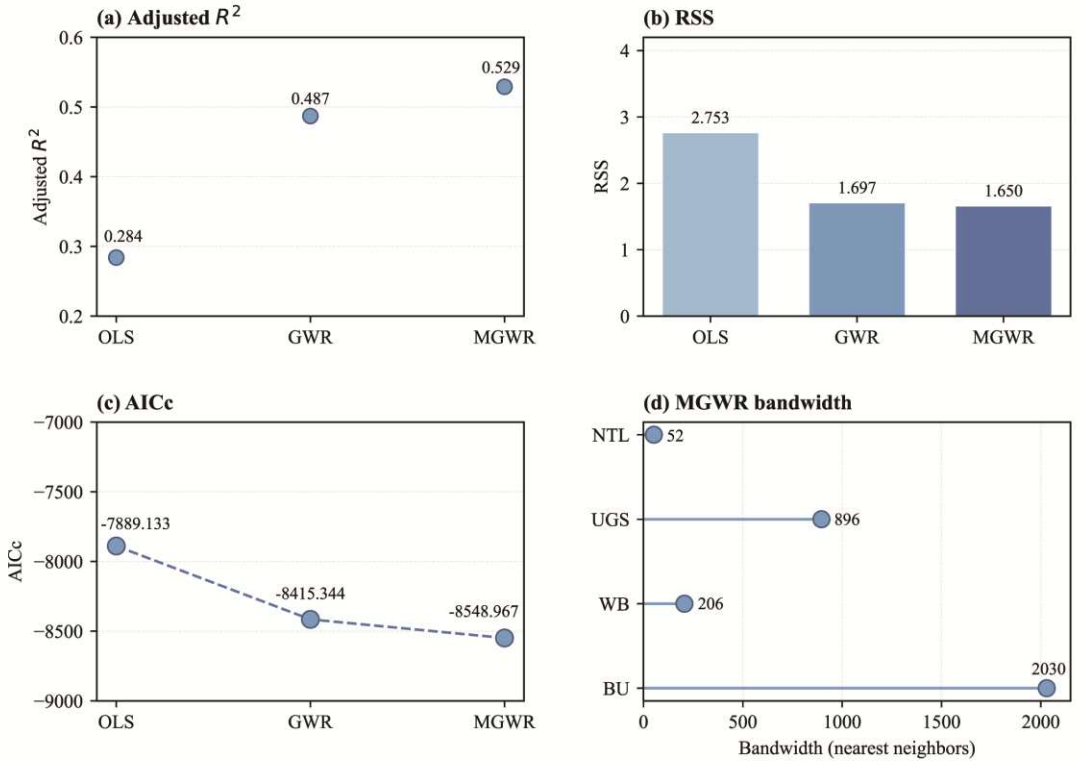
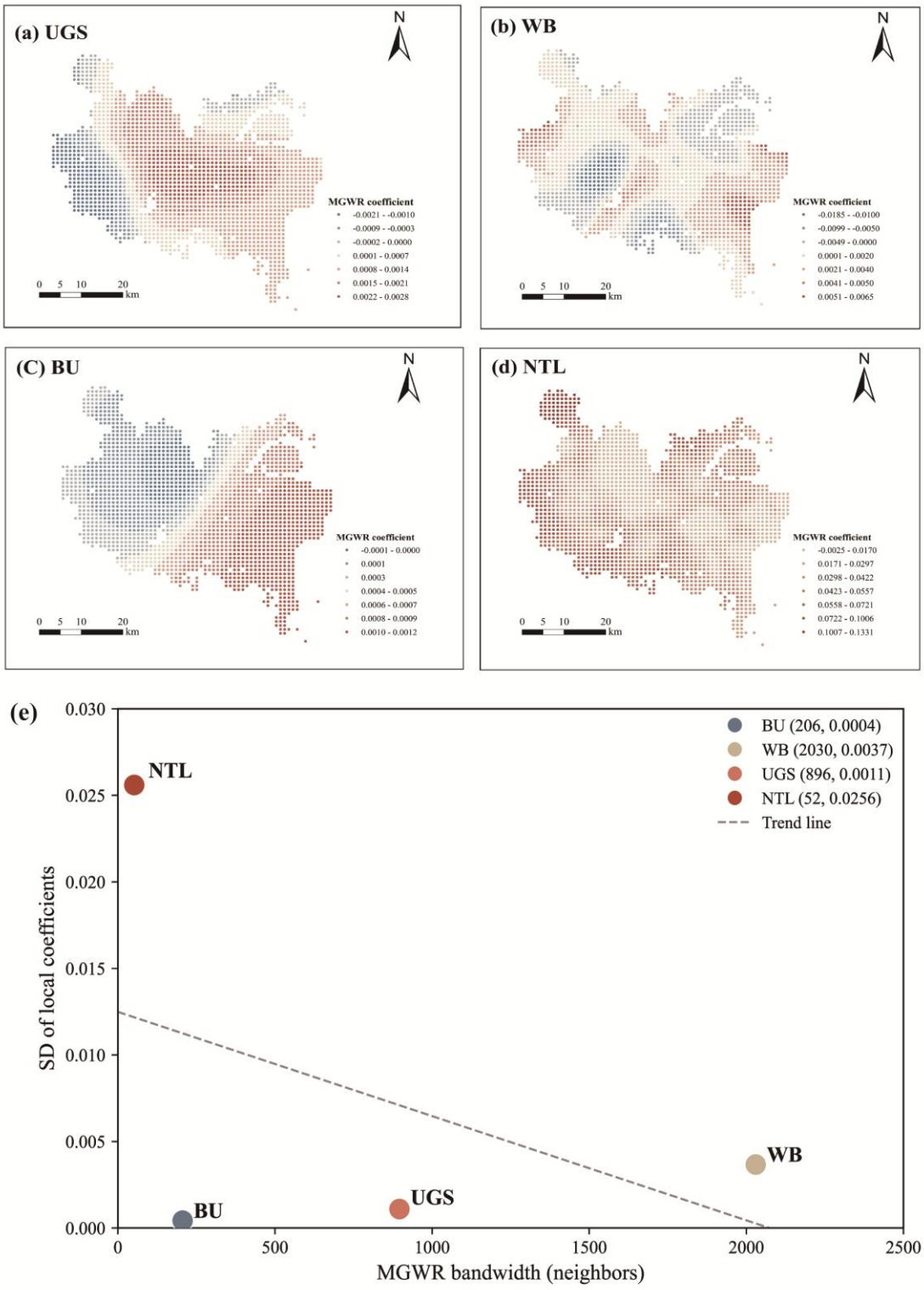


Fig.5.Spatial distribution of the explanatory variables


(a) Adjusted R^2
Adjusted R^2
0.6
0.5
0.4
0.3
0.2
0.284
0.487
0.529
OLS
GWR
MGWR
(b) RSS
RSS
4
3
2
1
0
2.753
1.697
1.650
OLS
GWR
MGWR
(c) AICc
AICc
−7000
−7500
−8000
−8500
−9000
-7889.133
-8415.344
-8548.967
OLS
GWR
MGWR
(d) MGWR bandwidth
NTL
52
UGS
896
WB
206
BU
2030
0
500
1000
1500
2000
Bandwidth (nearest neighbors)

516

517 Fig.6.Comparison of regressionmodels and multiscale spatial bandwidth



518

519 Fig.7.MGWR coefficients and bandwiths of variables

520 The spatial distributions of the MGWR local coefficients are shown in Fig. 7.
521 Unlike Fig. 5, which represents the spatial distribution of the explanatory variables

themselves, Fig.7 represents the spatially varying associations between each explanatory variable and RSHI.

The local coefficients of BU ranged from approximately −0.000103 to 0.001188. The coefficient surface showed a broad spatial transition, with positive coefficients more apparent in several eastern and southeastern urban areas, whereas negative or near-zero coefficients occurred in parts of the western and northern portions of the study area. This spatial variation is consistent with the near-zero global correlation between BU and RSHI ($r = -0.021$), suggesting that a single global coefficient may obscure spatially heterogeneous local associations.

The WB coefficients ranged from approximately −0.018464 to 0.006470 and displayed both negative and positive local values. Negative coefficients were concentrated in some areas associated with the major water-network structure, whereas positive or near-zero coefficients occurred elsewhere. The mixed coefficient signs indicate that the association between WB and RSHI was not spatially uniform across the study area.

UGS also exhibited spatially varying coefficient signs, with local coefficients ranging from approximately −0.002059 to 0.002817. Negative coefficients were more evident in some western areas, whereas positive coefficients occurred across several central and eastern areas. This pattern is consistent with the weak global correlation between UGS and RSHI ($r = 0.027$) and indicates that the overall near-zero correlation may partly reflect the spatial offsetting of local associations.

In contrast, NTL exhibited a predominantly positive coefficient pattern, with local coefficients ranging from approximately −0.002523 to 0.133058. The numerical range of the NTL coefficients was considerably wider than those of the other three predictors, and positive coefficients dominated most of the study area. This result is consistent with the relatively strong positive global correlation between NTL and RSHI ($r = 0.534$), while also indicating that the strength of this association varied spatially.

The MGWR bandwidths showed substantial differences among the explanatory variables (Fig. 6). BU had the largest bandwidth (2030 nearest neighbors), followed by UGS (896), WB (206), and NTL (52). Because these are adaptive nearest-neighbor bandwidths, they represent the number of neighboring observations used to estimate local relationships rather than fixed physical distances. Therefore, the bandwidths should be interpreted as indicators of the relative spatial scale of the fitted relationships rather than as direct cooling distances.

The large bandwidth of BU indicates that its association with RSHI was estimated over a relatively broad spatial context, whereas the smaller bandwidth of NTL indicates a more localized spatial scale. UGS occupied an intermediate-to-broad scale, while WB showed a relatively localized scale between UGS and NTL. The combination of local coefficient maps and variable-specific bandwidths therefore indicates that the explanatory variables differ in both the spatial pattern of their associations and the spatial scale over which these associations are estimated.

3.6. Sensitivity analysis of RSHI construction

To evaluate the robustness of the RSHI spatial pattern to alternative index specifications, three sensitivity scenarios were compared with the baseline 50:50 weighting scheme: a 60:40 weighting scheme, a 70:30 weighting scheme, and a reversed-NDWI scenario. Figure 8 illustrates the spatial distributions of the RSHI under these four specifications.

The spatial pattern under the 60:40 weighting scheme remained highly consistent with the baseline, with Pearson's correlation coefficient of 0.978 and Spearman's rank correlation coefficient of 0.977. The Jaccard similarity coefficient for high-RSHI zones was 0.803, while 86.41% of the baseline high-RSHI zones were retained. These results indicate that a moderate adjustment to the component weights had a limited effect on the overall spatial pattern and the identification of high-RSHI areas.

The RSHI under the 70:30 weighting scheme remained strongly correlated with the baseline, with a Pearson's correlation coefficient of 0.930 and a Spearman's rank correlation coefficient of 0.933. However, the Jaccard similarity coefficient decreased to 0.695, and the retention rate of baseline high-RSHI zones declined to 74.73%. This difference suggests that the broad spatial pattern was largely preserved, whereas the delineation of high-RSHI zones was more sensitive to changes in component weights.

In contrast, reversing the direction of NDWI produced a more substantial change in the index distribution. Pearson's and Spearman's correlation coefficients decreased to 0.406 and 0.481, respectively, while the Jaccard similarity coefficient and high-zone retention rate fell to 0.279 and 38.64%. This result indicates that the direction assigned to NDWI is an important determinant of the resulting composite index. Accordingly, the baseline RSHI should be interpreted in accordance with its specified component directions rather than as a direction-independent measure of surface heat conditions.

Overall, the sensitivity analysis demonstrates that the RSHI spatial pattern is relatively robust to moderate changes in component weights but is substantially affected by reversing the direction of NDWI. Because the highest RSHI class was identified separately for each specification using its own classification breaks, the overlap statistics describe the consistency of relative high-class locations rather than changes under a common absolute RSHI threshold.

Detailed spatial difference maps and supplementary statistics are provided in Fig. S1 and Tables S1-S2.

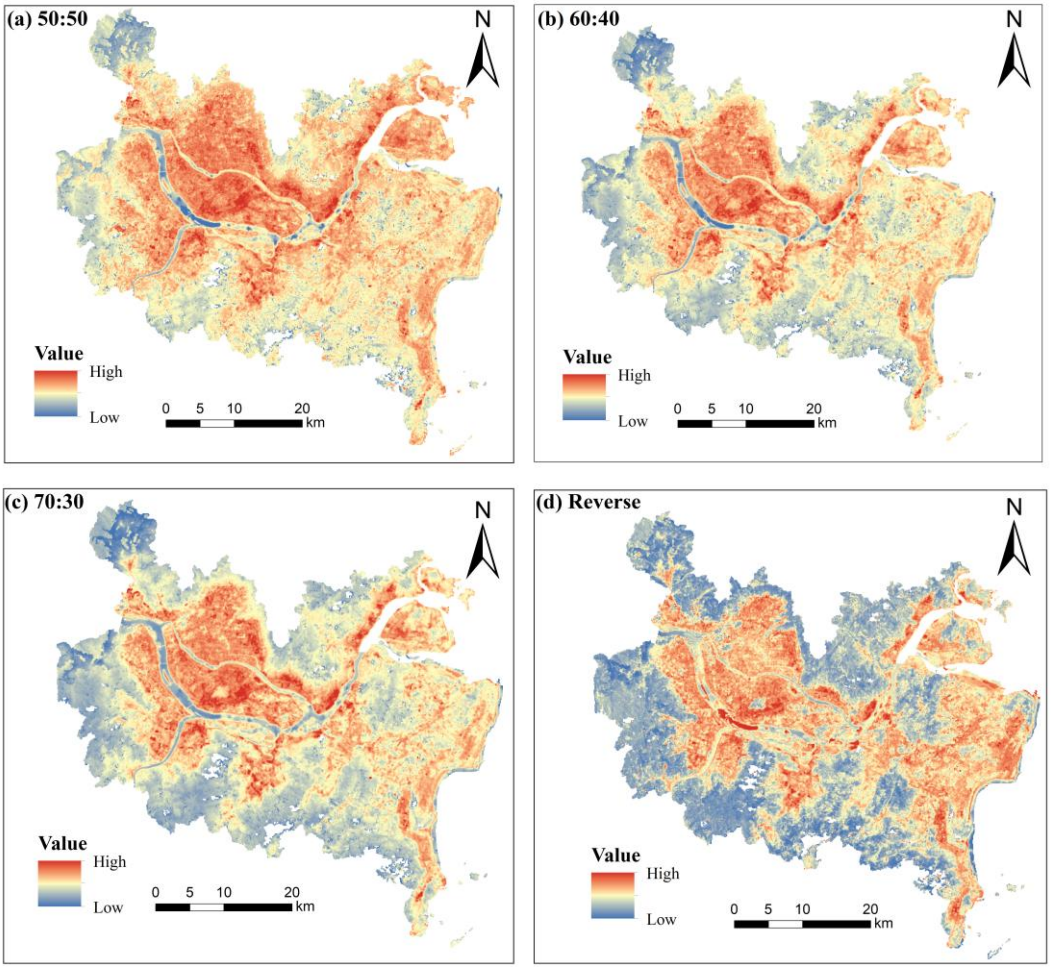


Fig. 8. Spatial distributions of the RSHI under alternative index specifications. (a) 50:50 weighting scheme; (b) 60:40 weighting scheme; (c) 70:30 weighting scheme; and (d) reversed-NDWI scenario.

4.Discussion

4.1 Spatial organization of surface thermal conditions

The spatial pattern of RSHI indicates that surface thermal conditions in the central urban area of Fuzhou were spatially differentiated rather than randomly distributed (Cai et al., 2019; Cai et al., 2024; Zheng et al., 2019). The concentration of RSHI in the intermediate classes, together with the localized occurrence of the lowest and highest classes, suggests that the study area was characterized by a continuous thermal gradient with spatially concentrated local extremes rather than a simple separation into uniformly hot and cool zones. This spatial organization is consistent with previous evidence that two- and three-dimensional urban landscape patterns can influence the spatial distribution of land surface temperature across cities of different sizes (Xu et al., 2023).

The spatial correspondence between high-RSHI areas and densely developed urban areas, as well as the spatial association of lower-RSHI areas with vegetation- and water-rich environments, is consistent with the role of urban land-cover composition in shaping surface thermal conditions. However, the global correlation results provide an important qualification. While NTL showed a moderate positive correlation with RSHI ($r = 0.534$), the global correlations of BU, WB, and UGS with RSHI were close to zero.

This apparent difference between spatial co-location and global correlation is important. For BU and UGS in particular, the local coefficient maps show both positive and negative associations across space, while their global correlations with RSHI are close to zero. This suggests that spatial aggregation can conceal local variation in the relationship between urban land cover and surface thermal conditions. The significant Moran's I (0.452, $p < 0.001$) further indicates that these local differences occur within a spatially structured system rather than as independent random variations.

The HH and LL patterns identified by LISA reinforce this interpretation. High-RSHI clusters were concentrated in highly developed urban contexts, whereas low-RSHI clusters were more commonly associated with ecological landscape contexts. Thus, the thermal pattern should be interpreted in relation to the surrounding landscape configuration rather than solely according to the land-cover type of an individual grid cell.

4.2 Multiscale heterogeneity of urban environmental associations

These findings complement previous MGWR-based analyses of Fuzhou's land surface temperature (LST). Yang et al. (2022) demonstrated that the relationships between LST and environmental factors were spatially heterogeneous and operated at different spatial scales. Building on this work, the present study examines the contrast between global associations and local relationships using RSHI, a composite indicator of relative surface thermal and moisture-related conditions. The results reveal distinct patterns across explanatory variables: NTL exhibited a clear positive global association with RSHI, whereas the global correlations for built-up land (BU), water bodies (WB), and urban green space (UGS) were close to zero. However, the MGWR coefficients for these three variables varied spatially and crossed zero across the study area, suggesting that global summary statistics alone may not adequately characterize their spatially varying relationships with RSHI.

NTL exhibited the clearest and most consistent positive association with RSHI across the global and local analyses. It had the strongest global correlation with RSHI ($r = 0.534$), remained positively associated with RSHI in the OLS model, and displayed predominantly positive local coefficients in the MGWR model. Its relatively small bandwidth of 52 nearest neighbors, compared with that of BU, further indicates that the NTL–RSHI relationship was estimated at a relatively localized spatial scale. Together, these results distinguish NTL from the other explanatory variables, whose global associations with RSHI were weak or nearly absent.

Nevertheless, the observed association should not be interpreted as direct evidence that nighttime human activity causes higher surface thermal conditions, particularly given the composite nature of RSHI.

For BU, the global correlation with RSHI was almost negligible ($r = -0.021$), whereas the MGWR coefficients ranged from −0.000103 to 0.001188. The coexistence of positive and negative local coefficients suggests that the near-zero global correlation may partly reflect spatial cancellation rather than a uniformly weak relationship. Previous studies have similarly reported that relationships between urban morphology and LST vary with spatial context and season (Li et al., 2021; Chen et al., 2022). The configuration of built-environment patches and their surrounding thermal context may also contribute to this heterogeneity (Ji et al., 2024). In addition, BU had a broad MGWR bandwidth of 2030 nearest neighbors, indicating that its relationship with RSHI was estimated over a broader spatial neighborhood than that of NTL. These findings suggest that the association between built-up land and RSHI cannot be adequately characterized by its global correlation alone.

UGS and WB showed a similar contrast between global and local results. Their global correlations with RSHI were close to zero ($r = 0.027$ for UGS and $r = 0.014$ for WB), while their MGWR coefficients varied substantially across space and changed sign across locations. The coefficients ranged from −0.002059 to 0.002817 for UGS and from −0.018464 to 0.006470 for WB. These patterns suggest that the relationships between RSHI and blue–green environmental features are spatially heterogeneous, and that positive and negative local associations may partly offset one another in global summaries. This interpretation is consistent with previous studies showing that the relationships between green and blue spaces and LST depend on spatial configuration, surrounding urban form, and analytical scale (Cai et al., 2022; Shen et al., 2022; Yu et al., 2023; Zhang et al., 2022; Yan et al., 2024). However, because RSHI combines surface temperature and moisture-related information, these results should not be interpreted as direct estimates of the cooling effects of green space or water bodies.

Overall, the findings highlight the value of combining global statistics with spatially explicit modelling to characterize urban environmental associations. Near-zero global correlations do not necessarily imply that a variable has uniformly weak local relationships with RSHI, while differences in MGWR bandwidths provide additional information about the spatial scales at which these relationships are estimated. The interpretation of these patterns should remain conditional on the construction of RSHI, the analytical scale, the selected explanatory variables, and the model specification. The results therefore provide evidence of spatially varying associations rather than definitive evidence of causal effects.

4.3 Implications for urban planning

The results suggest that urban thermal-environment management in Fuzhou may benefit from considering both spatial context and scale, rather than applying a uniform strategy across the entire urban area.

First, the broad bandwidth of BU indicates that relationships associated with built-up development are represented over a relatively broad neighborhood context. Therefore, analyses or interventions targeting built-up intensity may be more appropriately considered at the scale of connected urban districts or larger development zones rather than isolated land parcels.

Second, the intermediate-to-broad bandwidth of UGS indicates that vegetation-related associations extend across a broader spatial context than the more localized WB and NTL relationships. This supports the consideration of green-space connectivity and surrounding land-cover composition when evaluating the thermal role of vegetation, rather than focusing exclusively on the area of individual green patches.

Third, the relatively small bandwidth of WB suggests that water-related associations are more spatially localized. This is consistent with previous Fuzhou studies showing that waterbody cooling characteristics depend on patch and surrounding landscape conditions rather than being spatially uniform (Yao et al., 2022).

Finally, the small bandwidth and strong local variability of NTL indicate that areas with concentrated human activity may exhibit substantially different thermal associations over relatively short spatial contexts. This suggests that thermal-environment assessment based on human activity intensity may benefit from neighborhood-scale analysis rather than relying solely on city-wide averages.

Importantly, these implications should be interpreted as spatial planning considerations derived from observed associations, rather than direct causal prescriptions. The present cross-sectional analysis does not establish that changing any individual explanatory variable would produce a specific magnitude of change in RSHI.

4.4 Limitations and future research

Several limitations should be considered when interpreting the results.

First, the analysis was based on a single observation period in 2023. Consequently, the identified spatial relationships describe the thermal-environment pattern during the study period and cannot be assumed to remain constant across seasons or years. Multi-temporal observations would be required to determine whether the identified spatial scales are temporally stable.

Second, the analysis was conducted using a 1 km spatial unit. This scale provides a consistent framework for spatial regression but may smooth fine-scale variations in land cover, urban morphology, and thermal conditions. In particular, the MGWR bandwidths are defined as numbers of nearest-neighbor observations and should therefore not be interpreted directly as physical cooling distances.

Third, the explanatory variables did not include several potentially relevant urban morphological and meteorological factors, such as building height, sky-view factor, street-canyon geometry, wind conditions, and direct anthropogenic heat emissions. Their omission may contribute to unexplained spatial variation in RSHI.

Fourth, RSHI is a study-specific remote-sensing index constructed from surface thermal and moisture-related information. It characterizes relative surface thermal conditions and should not be interpreted as a direct measure of human thermal comfort, heat exposure, or health risk.

In addition, the RSHI was constructed using an equal-weight combination of normalized LST and NDWI, with both components retaining their original numerical directions. Although alternative weighting and directional scenarios were examined, the index remains a study-specific composite measure whose spatial pattern may depend on the selected components and their relative weights. Future research could evaluate alternative index specifications and validate their interpretation using independent surface or meteorological observations.

Finally, the analysis is observational and cross-sectional. Although the MGWR results identify spatially varying associations and variable-specific spatial scales, they do not establish causal relationships between the explanatory variables and RSHI. Future research could combine multi-temporal remote sensing observations with finer-scale urban morphology, meteorological measurements, and socioeconomic information to test the temporal stability and potential mechanisms underlying the observed multiscale relationships.

5.Conclusions

(1) The RSHI revealed pronounced spatial heterogeneity across the central urban area of Fuzhou, with values ranging from 0.236 to 0.910 and a mean of 0.648. High RSHI values were mainly concentrated in densely developed urban areas, where built-up land and nighttime light intensity were also spatially concentrated, whereas lower RSHI values were generally distributed around vegetation- and water-rich areas. This spatial correspondence indicates that the surface thermal environment is closely embedded in the underlying urban land-cover and human-activity structure rather than being spatially random. The significant positive Moran's I (0.452, $p < 0.001$) further confirms that high- and low-RSHI areas form spatially coherent clusters, with HH clusters mainly associated with highly urbanized areas and LL clusters concentrated around ecological spaces.

(2) The relationships between RSHI and individual explanatory variables cannot be adequately characterized by global correlations alone. Although the Pearson correlations between RSHI and BU, WB, and UGS were weak (−0.021, 0.014, and 0.027, respectively), NTL showed a comparatively stronger positive correlation with RSHI ($r = 0.534$). More importantly, the spatial coefficient maps revealed that these weak global relationships can conceal substantial local heterogeneity. This contrast demonstrates that spatially averaged relationships may obscure location-dependent effects, particularly for landscape variables whose thermal effects depend on their surrounding spatial context and configuration. The low VIF values (1.001-1.332) further indicate that this spatial heterogeneity was not primarily caused by severe multicollinearity among the explanatory variables.

(3) Model comparison revealed a progressive improvement from global to spatially varying and finally multiscale relationships. The adjusted R^2 increased from 0.284 for OLS to 0.487 for GWR and 0.529 for MGWR, while RSS decreased from 2.753 to 1.697 and 1.650, respectively; AICc also decreased from −7889.133 to −8415.344 and −8548.967. The improvement from OLS to GWR indicates that allowing coefficients to vary spatially substantially improves the representation of RSHI, whereas the additional improvement from GWR to MGWR indicates that spatial variation alone is insufficient: different explanatory variables operate over different spatial scales. Thus, the thermal environment of Fuzhou is better understood as a multiscale spatial system rather than a process governed by a single city-wide relationship.

(4) The MGWR results identified substantial differences in the estimated spatial scales of association among the explanatory variables. BU had the broadest adaptive bandwidth (2030 nearest neighbors), followed by UGS (896), WB (206), and NTL (52). These differences indicate that the associations between the explanatory variables and RSHI are represented at distinct spatial scales within the fitted model. The bandwidths describe model-estimated neighborhood scales rather than physical cooling distances, and their interpretation should remain within the scope of the cross-sectional analysis.

(5) Taken together, the results indicate that urban thermal conditions in Fuzhou emerge from the interaction of urban development intensity, blue-green landscape structure, and localized human activity, with each factor being associated with RSHI at a different spatial scale. The relatively broad scale of BU suggests that mitigation of development-related thermal accumulation may benefit from city- or district-scale consideration, whereas the more localized bandwidths of WB and NTL indicate that the thermal effects of blue spaces and concentrated human activity are more dependent on neighborhood-scale landscape context. UGS occupies an intermediate-to-broad spatial scale, implying that its thermal regulation is related not only to the amount of green space but also to its continuity and surrounding land-cover composition. This multiscale structure is consistent with previous research showing that the cooling effects of water bodies and green spaces depend on their spatial extent, configuration, and surrounding urban context.

(6) Overall, this study shows that the spatial distribution of RSHI and its associations with urban environmental characteristics cannot be fully described by global statistics alone. The combination of spatial autocorrelation analysis, global and local regression, and variable-specific bandwidth estimation provides a spatially explicit account of these relationships in the central urban area of Fuzhou. The findings support the consideration of spatial heterogeneity in urban surface-environment assessment, while further temporal analysis and independent validation are needed to establish the stability and broader applicability of the observed patterns.

CRediT authorship contribution statement

Mingxi Tian: Conceptualization, Methodology, Software, Formal analysis, Investigation, Data curation, Visualization, Writing-original draft. Yuanbin Cai: Supervision, Writing-review & editing. All authors have read and agreed to the published version of the manuscript.

Declaration of competing interest

The authors declare that they have no known competing financial interests or personal relationships that could have appeared to influence the work reported in this paper.

Acknowledgements

This research was funded by the Fuzhou University Zhicheng College Student Innovation and Entrepreneurship Training Program Project (2026045) and the Fujian Province Education Science Planning Routine Project for 2024 (FJJKBK24-018). The authors would like to thank the data providers for making the datasets used in this study publicly available.

Declaration of generative AI and AI-assisted technologies in the writing process

During the preparation of this manuscript, the authors used ChatGPT (OpenAI) to assist with language editing and improving the clarity and organization of the manuscript. After using this tool, the authors reviewed and edited the content as needed and take full responsibility for the content of the published work.

References

Ahn, Y., Tuholske, C., Parks, R.M., 2024. Comparing approximated heat stress measures across the United States. GeoHealth 8, e2023GH000923. https://doi.org/10.1029/2023GH000923.

Cai, Y., Chen, Y., Tong, C., 2019. Spatiotemporal evolution of urban green space and its impact on the urban thermal environment based on remote sensing data: A case study of Fuzhou City, China. Urban Forestry & Urban Greening 41, 333-343. https://doi.org/10.1016/j.ufug.2019.04.012.

Cai, Y., Gao, C., Pan, W., Chen, Y., Wu, Z., 2024. Research on optimal cooling landscape combination and configuration based on local climate zones—Fuzhou, China. Sustainability 16, 2367. https://doi.org/10.3390/su16062367.

Cai, Y.-B., Wu, Z.-J., Chen, Y.-H., Wu, L., Pan, W.-B., 2022. Investigate the difference of cooling effect between water bodies and green spaces: The study of Fuzhou, China. Water 14, 1471. https://doi.org/10.3390/w14091471.

Cai, Y.-B., Li, H.-M., Ye, X.-Y., Zhang, H., 2016a. Analyzing three-decadal patterns of land use/land cover change and regional ecosystem services at the landscape level: Case study of two coastal metropolitan regions, Eastern China. Sustainability 8, 773. https://doi.org/10.3390/su8080773.

Cai, Y.-B., Zhang, H., Zheng, P., Pan, W.-B., 2016b. Quantifying the impact of land use/land cover changes on the urban heat island: A case study of the natural wetlands distribution area of Fuzhou City, China. Wetlands 36, 285-298. https://doi.org/10.1007/s13157-016-0738-7.

Chen, J., Zhan, W., Du, P., Li, L., Li, J., Liu, Z., Huang, F., Lai, J., Xia, J., 2022. Seasonally

disparate responses of surface thermal environment to 2D/3D urban morphology. Building and Environment 214, 108928. https://doi.org/10.1016/j.buildenv.2022.108928.

Du, J., Xiang, X., Zhao, B., Zhou, H., 2020. Impact of urban expansion on land surface temperature in Fuzhou, China using Landsat imagery. Sustainable Cities and Society 61, 102346. https://doi.org/10.1016/j.scs.2020.102346.

Gao, Y., Zhao, J., Yu, K., 2022. Effects of block morphology on the surface thermal environment and the corresponding planning strategy using the geographically weighted regression model. Building and Environment 216, 109037. https://doi.org/10.1016/j.buildenv.2022.109037.

Guo, Q., Mistry, M.N., Zhou, X., Zhao, G., Kino, K., Wen, B., Yoshimura, K., Satoh, Y., Cvijanovic, I., Kim, Y., Ng, C.F.S., Vicedo-Cabrera, A.M., Armstrong, B., Urban, A., Katsouyanni, K., Masselot, P., Tong, S., Sera, F., Huber, V., Bell, M.L., Kyselý, J., Multi-Country Multi-City (MCC) Collaborative Research Network, Gasparrini, A., Hashizume, M., Oki, T., 2024. Regional variation in the role of humidity on city-level heat-related mortality. PNAS Nexus 3, pgae290. https://doi.org/10.1093/pnasnexus/pgae290.

He, J., Shi, Y., Xu, L., Lu, Z., Feng, M., 2024. An investigation on the impact of blue and green spatial pattern alterations on the urban thermal environment: A case study of Shanghai. Ecological Indicators 158, 111244. https://doi.org/10.1016/j.ecolind.2023.111244.

Ji, Y., Peng, Y., Tang, H., Li, Z., Xia, Y., Feng, T., 2024. How do heat waves affect the relationship between built environment patches of different compactness and land surface temperature? Building and Environment 266, 112044. https://doi.org/10.1016/j.buildenv.2024.112044.

Li, H., Li, Y., Wang, T., Wang, Z., Gao, M., Shen, H., 2021. Quantifying 3D building form effects on urban land surface temperature and modeling seasonal correlation patterns. Building and Environment 204, 108132. https://doi.org/10.1016/j.buildenv.2021.108132.

Lin, Z., Xu, H., Yao, X., Yang, C., Yang, L., 2023. Exploring the relationship between thermal environmental factors and land surface temperature of a “furnace city” based on local climate zones. Building and Environment 243, 110732. https://doi.org/10.1016/j.buildenv.2023.110732.

Luo, M., Lau, N., 2018. Increasing heat stress in urban areas of Eastern China: Acceleration by urbanization. Geophysical Research Letters 45. https://doi.org/10.1029/2018GL080306.

Ma, Y., Xu, C., Yang, Z., 2025. Quantifying the impact of urban blue-green spaces on humid-heat exposure risk: A case study of Nanjing’s central urban area. Ecological Indicators 176, 113708. https://doi.org/10.1016/j.ecolind.2025.113708.

Ndlovu, N., Nkeh Chungag, B., 2024. Impact of heat stress on cardiovascular health outcomes of older adults: A mini review. Aging and Health Research 4, 100189. https://doi.org/10.1016/j.ahr.2024.100189.

Oshan, T.M., Li, Z., Kang, W., Wolf, L.J., Fotheringham, A.S., 2019. mgwr: A Python implementation of multiscale geographically weighted regression for investigating process spatial heterogeneity and scale. ISPRS International Journal of Geo-Information 8, 269. https://doi.org/10.3390/ijgi8060269.

Potchter, O., Cohen, P., Lin, T.-P., Matzarakis, A., 2018. Outdoor human thermal perception in various climates: A comprehensive review of approaches, methods and quantification. Science of the Total Environment 631-632, 390-406. https://doi.org/10.1016/j.scitotenv.2018.02.276.

Rachid, A., Qureshi, A.M., 2023. Sensitivity analysis of heat stress indices. Climate 11, 181.

https://doi.org/10.3390/cli11090181.

Shen, Z.-J., Zhang, B.-H., Xin, R.-H., Liu, J.-Y., 2022. Examining supply and demand of cooling effect of blue and green spaces in mitigating urban heat island effects: A case study of the Fujian Delta urban agglomeration (FDUA), China. Ecological Indicators 142, 109187. https://doi.org/10.1016/j.ecolind.2022.109187.

Shi, S., Ji, S., Luo, Z., 2025. Spatial heterogeneity, interaction and multi-scale effects of driving factors of heat island intensity in different urban agglomerations. Sustainable Cities and Society 126, 106401. https://doi.org/10.1016/j.scs.2025.106401.

Wang, F., Gao, M., Liu, C., Zhao, R., McElroy, M.B., 2024. Uniformly elevated future heat stress in China driven by spatially heterogeneous water vapor changes. Nature Communications 15, 4522. https://doi.org/10.1038/s41467-024-48895-w.

Xiang, J., Bi, P., Pisaniello, D., Hansen, A., 2014. Health impacts of workplace heat exposure: An epidemiological review. Industrial Health 52, 91-101. https://doi.org/10.2486/indhealth.2012-0145.

Xu, D., Li, C., Hu, Y., Li, S., Kong, R., Zhang, Z., 2023. Quantifying the effects of 2D/3D urban landscape patterns on land surface temperature: A perspective from cities of different sizes. Building and Environment 233, 110085. https://doi.org/10.1016/j.buildenv.2023.110085.

Xu, D., Wang, Y., Zhou, D., Wang, Y., Zhang, Q., Yang, Y., 2024. Influences of urban spatial factors on surface urban heat island effect and its spatial heterogeneity: A case study of Xi'an. Building and Environment 248, 111072. https://doi.org/10.1016/j.buildenv.2023.111072.

Yan, Y., Hou, H., Murayama, Y., Wang, R., Hu, T., 2024. How do landscape patterns affect cooling intensity and scale? Evidence from 13 primary urban wetlands in China. Ecological Indicators 166, 112574. https://doi.org/10.1016/j.ecolind.2024.112574.

Yang, L., Yu, K., Ai, J., Liu, Y., Yang, W., Liu, J., 2022. Dominant Factors and Spatial Heterogeneity of Land Surface Temperatures in Urban Areas: A Case Study in Fuzhou, China. Remote Sensing 14, 1266. https://doi.org/10.3390/rs14051266.

Yao, X., Zhu, Z., Zeng, X., Huang, S., Liu, Q., Yu, K., Zhou, X., Chen, Z., Liu, J., 2022. Linking maximum-impact and cumulative-impact indices to quantify the cooling effect of waterbodies in a subtropical city: A seasonal perspective. Sustainable Cities and Society 82, 103902. https://doi.org/10.1016/j.scs.2022.103902.

Yu, H., Zhang, T., Fukuda, H., Ma, X., 2023. The effect of landscape configuration on outdoor thermal environment: A case of urban Plaza in Xi'an, China. Building and Environment 231, 110027. https://doi.org/10.1016/j.buildenv.2023.110027.

Zhang, Q., Zhou, D., Xu, D., Rogora, A., 2022. Correlation between cooling effect of green space and surrounding urban spatial form: Evidence from 36 urban green spaces. Building and Environment 222, 109375. https://doi.org/10.1016/j.buildenv.2022.109375.

Zheng, H., Chen, Y., Ding, W., Pan, W., Cai, Y., 2018. Characteristics of Land Surface Temperature Disturbance and Its Relationship to Built-up Land Expansion. Journal of Geo-Information Science 20(10), 1529-1540. https://doi.org/10.12082/dqxxkx.2018.180186.

Zheng, H., Chen, Y., Pan, W., Cai, Y., Chen, Z., 2019. Impact of land use/land cover changes on the thermal environment in urbanization: A case study of the natural wetlands distribution area in Minjiang River Estuary, China. Polish Journal of Environmental Studies 28, 3025-3041. https://doi.org/10.15244/pjoes/93743.

Zhou, Z., Nguyen-Xuan, T., Liao, H., Qiu, L., Im, E.-S., 2024. Characterization of temperature and humidity effects on extreme heat stress under global warming and urban growth in the Pearl and Yangtze River Deltas of China. Weather and Climate Extremes 44, 100659. https://doi.org/10.1016/j.wace.2024.100659.

Supplementary Files

This is a list of supplementary files associated with this preprint. Click to download.

- SupplementaryMaterials.docx